# Design Optimization of High-Torque BLDC Motors with Various Slot/Pole Combinations for Robotic Applications

Mohamed Y. Metwly, Landon Clark, Biyun Xie, JiangBiao He
Department of Electrical and Computer Engineering
University of Kentucky
Lexington, KY, USA
Email: mohamed.metwly@uky.edu

Abstract-Robots have been increasingly applied for harsh operating environments, such as disaster rescue, space exploration, and nuclear waste remediation. Robotic arms in such environments with extremely high/low temperatures and air pressure are prone to hardware failures, especially for joint motors and power electronic drives. Brushless DC (BLDC) motors are extensively used in robotic applications because they exhibit high reliability and efficiency. Thus, this paper presents a design optimization approach for high-torque BLDC motors for robotic applications to enhance the reliability and fault-tolerance capability based on a multi-objective genetic algorithm (MOGA). Owing to the inherent advantages of fractional-slot concentrated windings (FSCW) over distributed windings, this paper adopts BLDC motors with various slot/pole combinations. On the contrary, distorted flux distribution is one main drawback of FSCW, which may yield radial forces on the rotor. Moreover, the thermal behavior of the proposed slot/pole combinations is investigated, showing the resulting thermal stress. Finally, a broad comparison of the employed winding layouts is introduced to highlight the effect of the radial forces on the rotor deformation using finite element analysis (FEA). The higher the slot/pole combination, the higher the radial forces and rotor deformation.

Keywords—High-torque BLDC motors, robotic arm joint motors, multi-objective optimization, FSCW, collaborative robots

## I. INTRODUCTION

Since more and more robots are used in harsh environmental conditions, e.g., high temperature and high radiation, hardware failures in the joint motors and power electronic drives are likely to occur [1]. These failures may yield malfunction of the whole robot joints and cause much downtime costs. Thus, optimum design of joint motors is critical to improve system reliability for the robotic arms [2]. The electric motors used in robotic applications are brushless DC (BLDC) motors, servo motors, and stepper motors [3]. Servo motors offer high power density and efficiency; however, complex motor control and rotor sensory circuits are the main disadvantage with servo motors [4]. The high torque at low speed and the compact size are the main merits of stepper motors; however, lower high-speed torque is among the drawbacks of stepper motors [5]. BLDC motors are among the commonly utilized motors for robotic applications. For instance, seven BLDC joint motors are adopted by the Kinova Gen3 robotic arm [6]. Thus, BLDC motor drives are selected in this work owing to their high torque-producing capability, high robustness, and high efficiency.

This material is based upon work supported by the U.S. National Science Foundation (NSF) under Grant No. 2205292.

BLDC motors can be equipped with conventional distributed windings or fractional-slot concentrated windings (FSCW). Nevertheless, FSCW offers numerous merits over their distributed counterparts, such as short-end turns, high slot fill factor, and low cogging torque [7]. On the other hand, the main drawback of FSCW is the distorted air gap flux distribution, which yields radial forces on the rotor. In the literature, various FSCW slot/pole combinations have been introduced [8]. The employed slot-pole combination highly affects the air gap magnetic field and the resulting radial forces on the rotor. In [9], the design of a 12-slot/10-pole permanent magnet (PM) motor and a Vernier motor with two air gaps is discussed for collaborative robot applications. It is concluded that the Vernier motor exhibits higher torque, albeit at higher winding losses.

Compared to high-speed BLDC motors at which high frequency and high switching losses may affect the motor-drive performance, low-speed BLDC motors have design challenges, such as high torque ripple that may cause significant noise and vibration [10] and high radial forces that may lead to rotor deformation. The design optimization of high-torque motors has been presented in the recent literature for numerous applications [11-13]. A design optimization approach of high-power BLDC motors has been introduced for marine propulsion applications [13]. A novel circular winding BLDC motor is proposed, at which the circularly connected windings and their commutation make it adequate for high-power applications. In that case, electromagnetic weight, cogging torque, copper loss, and torque ripple constitute the four optimization objectives to maximize the torque density and minimize the vibrations. Moreover, the design of a high-torque BLDC motor has been presented for robotic arm joint motors [11].

In addition to electromagnetic analysis, thermal analysis and mechanical modeling are important for the design of electric motors [14]. In [15], a magneto-thermal analysis of a high-torque BLDC motor has been proposed for humanoid robots' joint motors. This study aimed at achieving a high-torque low-mass motor while minimizing the temperature rise in the motor. Furthermore, the thermal analysis of low-speed high-torque FSCW-based PM motors has been investigated [16]. The machine efficiency has been improved considering the electromagnetic and thermal analysis based on the analytical magnetic equivalent circuit model and finite element analysis (FEA). The magnetic radial forces and deformation in the rotor have been presented in the literature for high-speed applications [17, 18]. However, only a few studies have been

found in the literature for high-torque low-speed applications. In [19], the effect of the radial magnetic forces on the BLDC motor deflections has been highlighted, showing that even micrometer deformation can yield vibrations and noise during the motor operation. In that case, the magnetic forces based on 3D electromagnetic FE simulations are coupled to the 3D structural FE model to verify the efficacy of proposed analytical model to estimate the deformation. Finally, the radial forces are studied to define the dominant space and time force harmonics.

In this paper, a high-torque BLDC motor will be optimally designed for robotic applications based on a multi-objective genetic algorithm (MOGA), considering the average torque, peak-to-peak torque ripple, and core losses as the optimization objectives. The performance of a three-phase surface-mounted permanent magnet (SPM) machine with several slot/pole combinations has been investigated using FEA. The main contributions of this study are summarized as follows:

 Develop a design optimization framework of BLDC motors with numerous slot/pole combinations, i.e., 12-slot/10-pole, 24-slot/22-pole, and 36-slot/34-pole, highlighting the optimum trade-off among the abovementioned performances.

Optimal

40

 $T_{rip}, N_m$ 

60

10

T 75

- Study the impacts of the employed FCSW-based slot/pole combinations on the BLDC motor thermal, mechanical, and electromagnetic performances using intensive FE simulations.
- Consider the deformation in the rotor due to radial forces in low-speed BLDC motors, which has not been conceived thus far.

# II. BLDC DESIGN OPTIMIZATION APPROACH

In this study, three-phase SPM motors with three slot/pole combinations, namely, 12-slot/10-pole, 24-slot/22-pole, and 36-slot/34-pole, have been designed. The proposed winding configurations and their MMF harmonic spectra are shown in Figs. 1 and 2, respectively. Torque-producing component and dominant slot harmonics are depicted for the three slot/pole combinations, e.g., the fifth harmonic (h = 5) and the seventh harmonic (h = 7) are the torque-producing components and slot harmonics, respectively, when the 12-slot/10-pole machine is employed. In that case, the 5<sup>th</sup>, 11<sup>th</sup>, and 17<sup>th</sup> harmonic components are the main torque production components. Whereas, the 7<sup>th</sup>, 13<sup>th</sup>, and 19<sup>th</sup> harmonic components mainly contribute to the induced rotor eddy current losses.

75

65

10

20

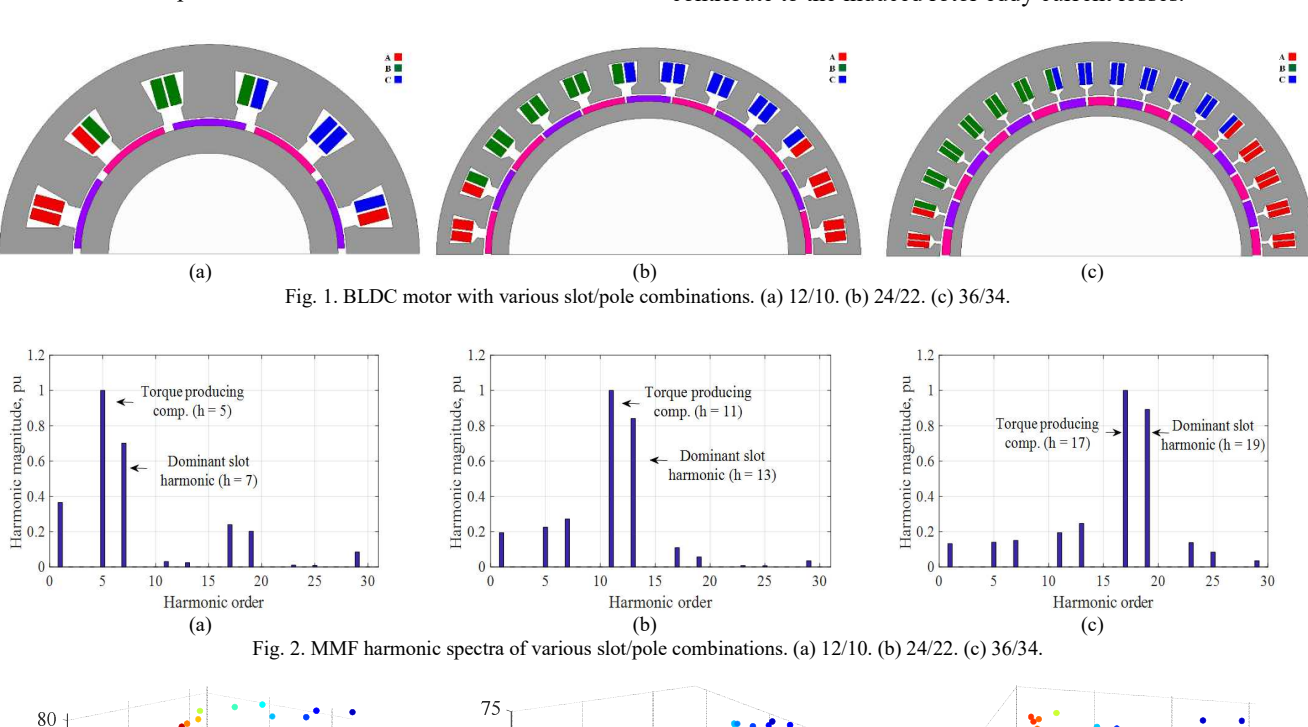
30

Nm

Optimal

40

20



(b) Fig. 3. Optimization results of various slot/pole combinations using FEA. (a) 12/10. (b) 24/22. (c) 36/34.

 $P_{1a}^{18}, W$ 

Optimal

T avg, Nm

65

20

20

15

 $P_{loss}$ , W

The proposed SPM-based BLDC motors with FSCW windings are first designed based on the sizing equation [20] and further optimized based on the FEA using MOGA. Performance-wise, it is crucial to maximize the average torque and minimize the peak-to-peak torque ripple and core losses. High-torque capability is crucial in certain robotic applications to carry heavy objects. Torque ripple is the main cause of vibrations and noise in SPM motors, while high core losses may yield thermal demagnetization. Thus, the objective function (1) is formulated to achieve the above-mentioned targets. The magnet thickness  $Y_m$ , slot-opening ratio  $t_{so}/\tau_{so}$ , and permanent magnet (PM) width to pole pitch ratio  $\alpha_{PM}$  are the decision variables. Their variation ranges are [2.5-4.5 mm], [0.1-0.3], and [0.75-0.9] respectively. Moreover, the objective function is minimized considering several inequality constraints, e.g., current density J, slot fill factor  $K_{cu}$ , and lower and upper bounds of the decision variables  $(X_i^{min} \text{ and } X_i^{max})$ . It is worth mentioning that the cooling technique determines the current density, and the slot fill factor is adjusted to enhance the effective machine winding turns and thus the torque density.

minimize

$$Y_{m}, \frac{t_{so}}{\tau_{so}}, \alpha_{PM} \qquad F(X_{i})$$

$$F(X_{i}) = \lambda_{1} \frac{T'_{avg}}{T_{avg}(X_{i})} + \lambda_{2} \frac{T_{rip}(X_{i})}{T'_{rip}} + \lambda_{3} \frac{P_{loss}(X_{i})}{P'_{loss}}$$

$$(1)$$

Subject to 
$$J \leq 4 \, A/mm^2 \\ K_{cu} \leq 0.4 \, \% \\ T_{avg} \geq 70 \, Nm \\ X_i^{min} \leq X_i \leq X_i^{max}$$
 (2)

where  $T_{avg}(X_i)$ ,  $T_{rip}(X_i)$ , and  $P_{loss}(X_i)$  are the average torque, torque ripple, and core losses, respectively. Their initial values are  $T'_{avg}$ ,  $T'_{rip}$ , and  $P'_{loss}$ , respectively. Besides, the optimization objectives are of equal priority by using equal weighting factors,  $\lambda_1$ ,  $\lambda_2$ , and  $\lambda_3$ , whereas  $\lambda_1 + \lambda_2 + \lambda_3 = 1$ . Even though the values of the weighting factors are critical to the optimization objectives, there is no standard so far to define these factors [14].

In order to address the inherent conflict between the optimization objectives, a MOGA-based optimization strategy has been employed to determine the optimal operating point. This point represents the best trade-off between the three objectives. In this paper, only high-sensitive parameters are optimized using the proposed approach. The relevant parameters of the optimization approach are as follows: the space dimension is 3, the population consists of 50 individuals, each dimension is divided into 50 divisions, the mutation probability is 0.2, the crossover value is set to 0.25, and the stopping criteria is the maximum number of generations, i.e., 100. The optimization results are shown in Fig. 3, in which the optimal design is highlighted in red. Finally, Tables I and II show the motor design specifications and optimal parameters, respectively.

# III. SIMULATION RESULTS

In order to verify the proposed design optimization approach, simulations have been carried out on a BLDC motor equipped with three slot/pole combinations for robotic applications using the ANSYS Workbench.

TABLE I. BLDC MOTOR DESIGN RATINGS.

Power (W)	1000
Rated speed (rpm)	125
Rated torque (Nm)	73
DC link voltage (V)	48
Electric loading (A/mm)	15

TABLE II. BLDC Motors' Design Parameters.							
Slot/pole combination	12/10	24/22	36/34				
Stator outer diameter (mm)	255.6	226	216.6				
Stator inner diameter (mm)	166.6	164.6	163				
Stack length (mm)	165.6	164.6	164.5				
Air gap length (mm)		1					
Stator back iron height (mm)	15	7.4	4.9				
Magnet thickness (mm)	4	4.1	4.3				
No. of turns per coil	17	8	5				
Line current peak value (A)	28.6	30	31.9				

The same magnetic flux density, electric loading, copper fill factor, and stack length to air gap diameter ratio are selected for fair comparison between the three winding layouts. The three motor designs are simulated at the rated conditions, and their 2D electromagnetic FE results are given in Figs. 4-6. Fig. 4 shows the flux density distributions of the three slot/pole combinations. It can be seen that the flux density in the stator tooth tips and rotor yoke does not exceed the required value of 1.8 T in the three motors, which alleviates the risk of magnetic saturation.

The torque profiles of the BLDC motor with three winding configurations are shown in Fig. 5. The same average torque can be achieved by the three slot/pole combinations with a slight improvement when the 10-pole machine is employed. However, the torque ripple is considerably reduced with higher slot/pole combinations, e.g., the torque ripple is 26 Nm, 35 Nm, and 56 Nm when the 34-pole, 22-pole, and 10-pole motors are used, respectively. The optimal design outperforms its initial counterpart for the three motors, i.e., the peak-to-peak torque ripple is reduced from 56 Nm to 40 Nm for the 12-slot/10-pole winding layout. The same conclusion can be drawn for the 24-slot/22-pole and 36-slot/34-pole winding configurations.

The radial forces are high in the proposed low-speed hightorque BLDC motor for robotic applications, and their effect on the rotor deformation is also presented in this paper. Basically, radial forces are the forces between the stator and rotor due to the produced flux in the air gap and are defined as the integration of the magnetic flux density squared over the permeability. In FSCW, the flux distribution is distorted, which is one main drawback of the FSCW topology. Therefore, the radial forces tend to be high and may yield a reduction in the motor lifetime and eccentricity in the long run [14]. The electromagnetic forces are calculated using the Maxwell Stress Tensor. Fig. 6 depicts the electromagnetic radial forces for the proposed three slot/pole combinations. The higher the slot/pole combination, the higher the radial forces.

Finally, Table III lists the comparison of the proposed winding configurations with respect to the output torque, torque ripple, phase voltage, and core losses. The core losses keep increasing with the high number of poles owing to the rise in the fundamental frequency. For instance, the stator core loss is 13 W, 16 W, and 19.8 W when the 10-pole, 22-pole, and 34-pole motors are utilized, respectively.

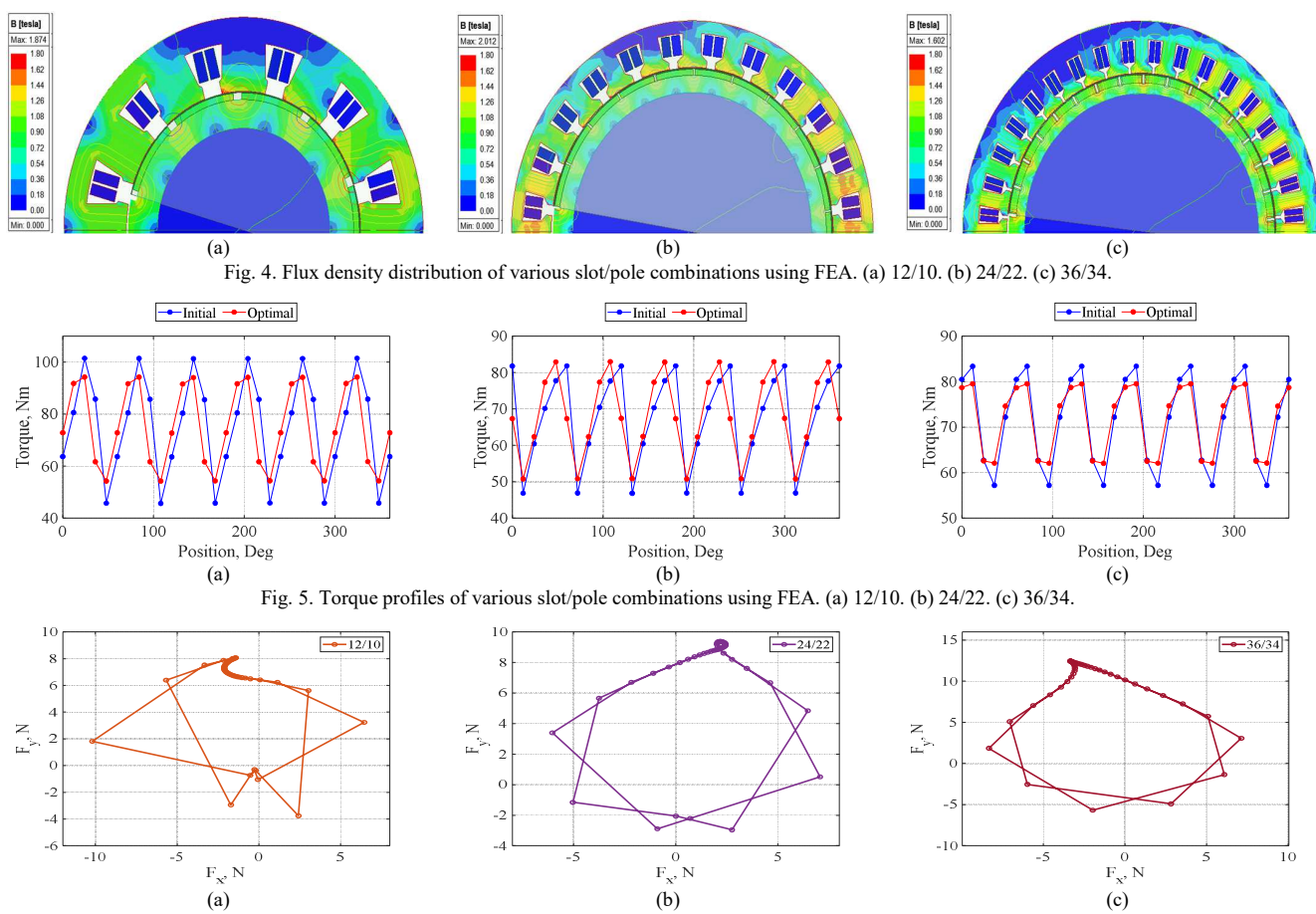


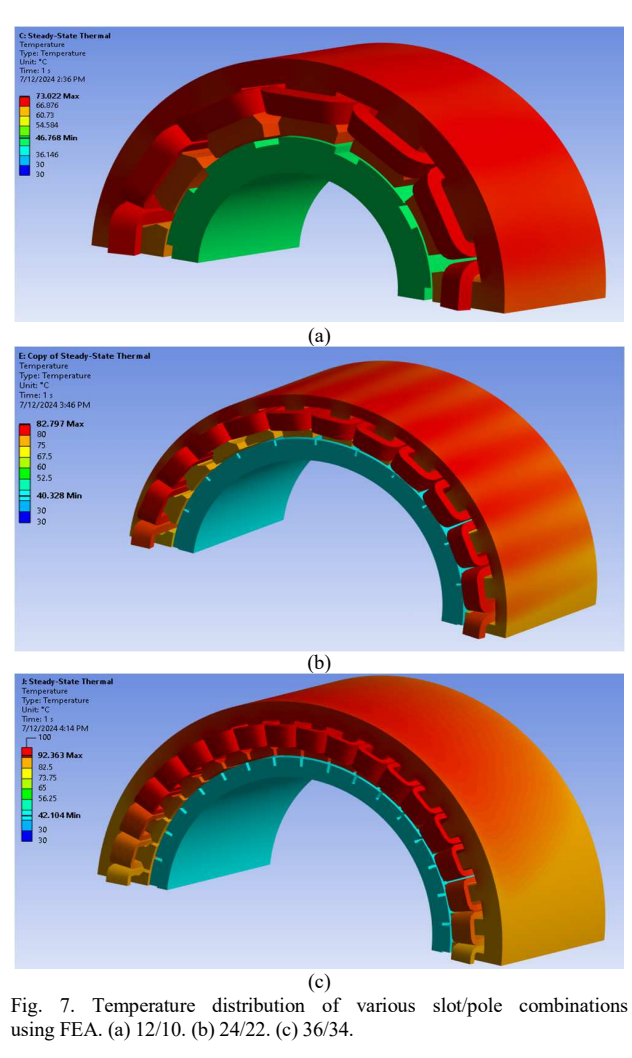
Fig. 6. Radial forces of various slot/pole combinations using FEA. (a) 12/10. (b) 24/22. (c) 36/34.

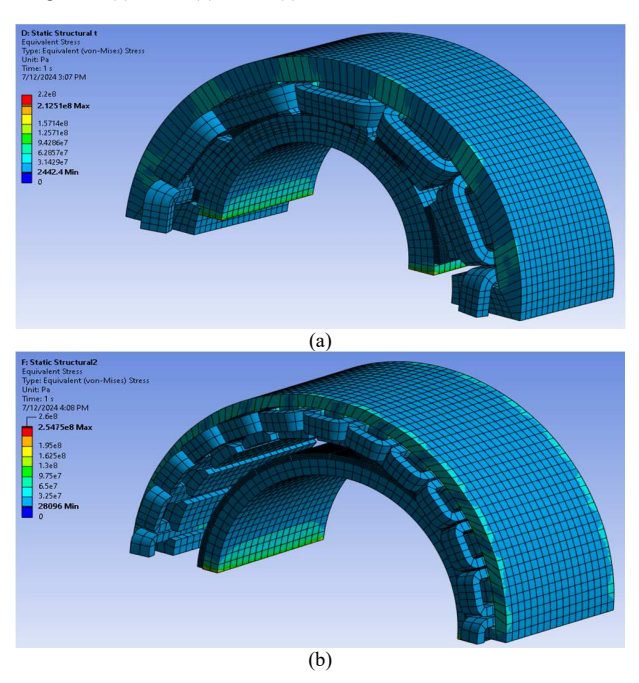
TABLE III. QUANTITATIVE ANALYSIS OF THE SIMULATION RESULTS.

Output	12-slot/10-pole		24-slot/22-pole		36-slot/34-pole	
	Initial	Optimal	Initial	Optimal	Initial	Optimal
Average torque (Nm)	73.12	75	67	70	71	72
Peak-to-peak torque ripple (Nm)	56	40	35	30	26	17
Phase-A back EMF (Vrms)	20.82	20.82	19.11	19.11	19.73	19.73
Stator core loss (W)	13	11	16	14	19.8	16
Rotor core loss (W)	0.756	0.127	0.976	0.829	1.476	1.129
Permanent magnet loss (W)	4.35	3.46	0.72	0.27	0.4	0.17

To further evaluate the performance of the proposed winding layouts for robotic applications, thermal and mechanical analyses have been performed in this paper using the Ansys Workbench. First, the core losses are calculated using 3D electromagnetic simulations. After that, the losses are coupled to the steady-state thermal analysis to measure the temperature distribution. The temperature distributions of the three slot/pole combinations are shown in Fig. 7. It is clear that the winding temperature is the highest one since the cooper losses are dominant in the motors. In that case, the ambient temperature is set to 40 °C. The temperature increases with the slot/pole combination because the losses are higher, as highlighted in Table III. For instance, the maximum temperature is 73 °C in the motor with slot/pole of 12/10 compared to the scenario at 92 °C in the motor with slot/pole of 36/34 configuration.

Moreover, the temperature distributions are coupled to the 3D structural FE simulations to measure the stress distribution in the proposed winding layouts. Fig. 8 illustrates the stress distribution of the various slot/pole combinations. The stress distributions are proportional to the temperature distributions, i.e., the higher the temperature, the higher the thermal stress. This is proved since the equivalent stress keeps rising with the higher slot/pole combinations, i.e., the equivalent stress is 212 MPa, 254 MPa, and 277 MPa when the 10-pole, 22-pole, and 34-pole motors are utilized, respectively. It should be noted that the equivalent stress for the proposed winding configurations is below the yield strength of the core and magnet materials, i.e., the yield strength of the M250-35A used in stator and rotor is 455 mPa and the N42UH used in the magnets is 285 MPa. This shows that the risk of the material undergoing plastic deformation is mitigated.





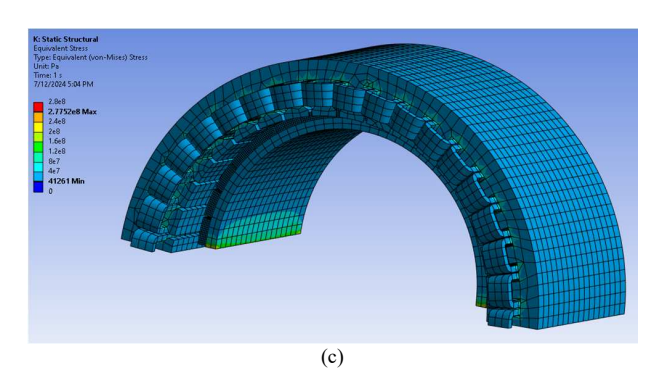
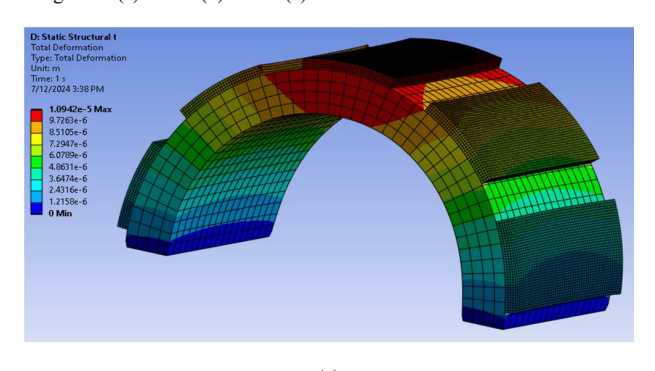
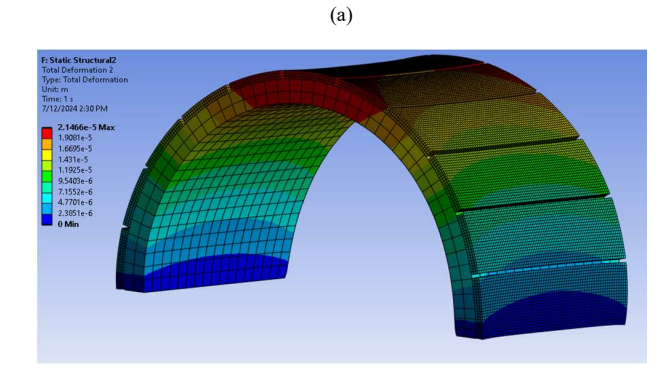


Fig. 8. Stress distribution of various slot/pole combinations using FEA. (a) 12/10. (b) 24/22. (c) 36/34.





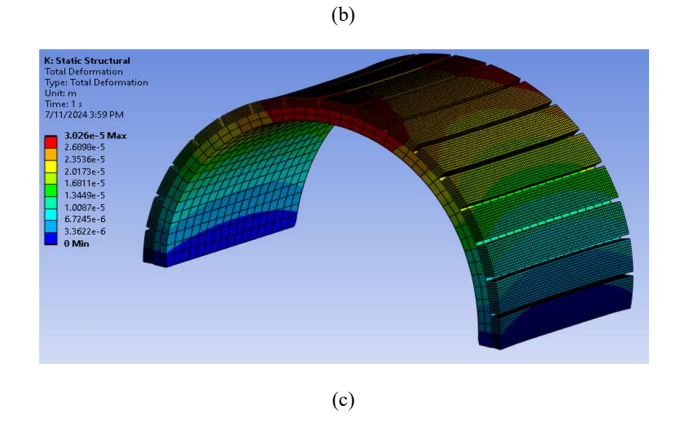


Fig. 9. Total deformation in the rotor of various slot/pole combinations using FEA. (a) 12/10. (b) 24/22. (c) 36/34.

Finally, the rotor deformation is calculated using the 3D structural FEA based on the electromagnetic radial forces and stress distributions. The total deformation in the rotor for the three slot/pole combinations is shown in Fig. 9. The higher the slot/pole combination, the higher the total deformation, e.g., the 10-pole, 22-pole, and 34-pole machines exhibit 10.9  $\mu m$ , 21.4  $\mu m$ , and 30.2  $\mu m$  total deformation, respectively. These deformations can result in certain vibrations and acoustic noise during the motor operation.

## IV. CONCLUSION

This paper presents a design optimization approach for SPMbased BLDC motors for robotic arms using MOGA optimization. A thorough comparative analysis of three-phase BLDC motors equipped with FSCW 12/10, 24/22, and 36/34 slot/pole combinations has been introduced using the FEA. The higher the slot/pole combination, the lower the torque ripple and motor mass; thus, the higher the gravitational power density. Finally, thermal behavior and rotor deformation due to radial forces have been investigated using Ansys Workbench. Even though the electromagnetic performances of the motors are enhanced when the higher slot/pole combination is adopted, the thermal and stress distributions are increased, resulting in higher rotor deformation. It can be concluded that the higher the slot/pole combination, the better the electromagnetic performances, but probably the worse the thermal and mechanical performances.

### REFERENCES

- [1] G. Chen, L. Li, Y. Fu, B. Yuan, and J. Fei, "Halt Optimization Strategy for a Space Manipulator with a Joint-Locked Failure," *International Journal of Aerospace Engineering*, vol. 2020, 2020, doi: https://doi.org/10.1155/2020/8811433.
- [2] Z. Yin, N. Hu, J. Chen, Y. Yang, and G. Shen, "A review of fault diagnosis, prognosis and health management for aircraft electromechanical actuators," *IET Electric Power Applications*, vol. 16, no. 11, pp. 1249-1272, 2022.
- [3] S. B. Niku, Introduction to robotics: analysis, systems, applications. Prentice hall New Jersey, 2001.
- [4] S. Sakama, Y. Tanaka, and A. Kamimura, "Characteristics of Hydraulic and Electric Servo Motors," in *Actuators*, 2022, vol. 11, no. 1: MDPI, p. 11.
- [5] M. Quigley, A. Asbeck, and A. Ng, "A low-cost compliant 7-DOF robotic manipulator," in 2011 IEEE International Conference on Robotics and Automation, 2011: IEEE, pp. 6051-6058.
- [6] B. Xie and A. A. Maciejewski, "Maximizing the probability of task completion for redundant robots experiencing locked joint failures," *IEEE Transactions on Robotics*, vol. 38, no. 1, pp. 616-625, 2021.

- [7] A. M. El-Refaie, "Fractional-slot concentrated-windings synchronous permanent magnet machines: Opportunities and challenges," *IEEE Transactions on industrial Electronics*, vol. 57, no. 1, pp. 107-121, 2009.
- [8] E. Carraro, N. Bianchi, S. Zhang, and M. Koch, "Design and performance comparison of fractional slot concentrated winding spoke type synchronous motors with different slot-pole combinations," *IEEE Transactions on Industry Applications*, vol. 54, no. 3, pp. 2276-2284, 2018.
- [9] M.-T. Duong, T.-P. Luu, T. D. Do, and Y. Perriard, "Design of High Torque Density Permanent Magnet Motors and Drives for Collaborative Robot Applications," in 2021 24th International Conference on Electrical Machines and Systems (ICEMS), 2021: IEEE, pp. 1060-1064.
- [10] C.-L. Huang, F.-C. Lee, C.-J. Liu, J.-Y. Chen, Y.-J. Lin, and S.-C. Yang, "Torque ripple reduction for blde permanent magnet motor drive using de-link voltage and current modulation," *IEEE Access*, vol. 10, pp. 51272-51284, 2022.
- [11] Q. Hua et al., "Design of a High-torque Robot Joint and Its Control System," in *Journal of Physics: Conference Series*, 2022, vol. 2281, no. 1: IOP Publishing, p. 012007.
- [12] R. Mizutani and N. Matsui, "Optimum design approach for low-speed, high-torque permanent magnet motors," *Electrical Engineering in Japan*, vol. 135, no. 4, pp. 52-63, 2001.
- [13] Q. Zhang, S. Cheng, D. Wang, and Z. Jia, "Multiobjective design optimization of high-power circular winding brushless DC motor," *IEEE Transactions on Industrial Electronics*, vol. 65, no. 2, pp. 1740-1750, 2017.
- [14] A. Hemeida, M. Y. Metwly, A. S. Abdel-Khalik, and S. Ahmed, "Optimal design of a 12-slot/10-pole six-phase SPM machine with different winding layouts for integrated on-board EV battery charging," *Energies*, vol. 14, no. 7, p. 1848, 2021.
- [15] W. Zhang, Z. Yu, X. Chen, and Q. Huang, "The magneto-thermal analysis of a high torque density joint motor for humanoid robots," in 2018 IEEE-RAS 18th International Conference on Humanoid Robots (Humanoids), 2018: IEEE, pp. 112-117.
- [16] Y. Huang, Z. Zhu, B. Guo, H. Lin, and S. Fang, "Design and thermal analysis on high torque low speed fractional-slot concentrated windings in-wheel traction motor," in 2016 XXII international conference on electrical machines (ICEM), 2016: IEEE, pp. 1487-1492.
- [17] Y. Li, Y. Pei, Z. Song, and F. Chai, "Effect of rotor deformation on magnetic radial force in interior permanent magnet synchronous motors with V-shaped rotor structures," in *IECON 2016-42nd Annual Conference* of the *IEEE Industrial Electronics Society*, 2016: IEEE, pp. 1906-1911.
- [18] M. E. Gerlach, M. Zajonc, and B. Ponick, "Mechanical stress and deformation in the rotors of a high-speed PMSM and IM= Mechanischer Stress und Verformung in den Rotoren einer Hochdrehzahl-PMSM und einer Hochdrehzahl-IM," *Elektrotechnik und Informationstechnik 138* (2021), Nr. 2, vol. 138, no. 2, pp. 96-109, 2021.
- [19] S. Leitner, N. Saed, and A. Muetze, "Analysis of claw deflections and radial magnetic forces in low-cost sub-fractional horsepower BLDC clawpole motors," in 2021 IEEE Energy Conversion Congress and Exposition (ECCE), 2021: IEEE, pp. 3909-3914.
- [20] S. Huang, J. Luo, F. Leonardi, and T. A. Lipo, "A general approach to sizing and power density equations for comparison of electrical machines," *IEEE Transactions on Industry Applications*, vol. 34, no. 1, pp. 92-97, 1998.